Large-Area Bernal-Stacked Bi-, Tri-, and Tetralayer Graphene

Zhengzong Sun,[†] Abdul-Rahman O. Raji,[†] Yu Zhu,[†] Changsheng Xiang,[†] Zheng Yan,[†] Carter Kittrell,[‡] E. L. G. Samuel,[†] and James M. Tour*[,†,‡,§]

[†]Department of Chemistry, [‡]Richard E. Smalley Institute for Nanoscale Science and Technology, [§]Department of Mechanical Engineering and Materials Science, Rice University, 6100 Main Street, Houston, Texas, 77005

ABSTRACT Few-layer graphene, with Bernal stacking order, is of particular interest to the graphene community because of its unique tunable electronic structure. A synthetic method to produce such large area graphene films with precise thickness from 2 to 4 layers would be ideal for chemists and physicists to explore the promising electronic applications of these materials. Here, large-area uniform Bernal-stacked bi-, tri-, and tetralayer graphene films were successfully synthesized on a Cu surface in selective growth windows, with a finely tuned total pressure and CH_4/H_2 gas ratio. On the basis of the analyses obtained, the growth mechanism is not an independent homoexpitaxial layer-by-layer growth, but most likely a simultaneous-seeding and self-limiting process.

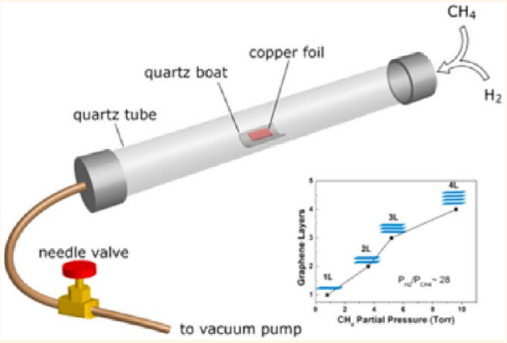

KEYWORDS: graphene · graphene mechanism · Bernal · bilayer · few-layer · chemical vapor deposition · copper

Parameters for the chemical vapor deposition (CVD) growth of graphene have been explored on different metal catalysts.[1−3] Since the discovery of Cu-based graphene growth,[1] the preparation of high-quality uniform large-area graphene monolayers becomes feasible. Multilayer graphene films with specific stacking orders have attracted enormous attention due to their tunable electronic structures.[4−7] Until recently, most of these experiments were based on micrometer-sized multilayer exfoliated graphene flakes,[4−7] requiring a tedious process that is difficult to scale. To solve this challenge, here we demonstrate consistent CVD growth windows for large-area Bernal-stacked bi-, tri-, or tetralayer graphene on Cu surfaces.

Parameters that could affect the thickness of graphene growth include the pressure in the system, gas flow rate, growth pressure (the partial pressure of both the growth gas and the carrier gas), growth temperature, and cooling rate.[8−11] On the basis of previous CVD growth conditions for monolayer, bilayer, and multilayer graphene summarized in the Supporting Information, Table S1, we hypothesized that the partial pressure of both the carbon sources and the H_2 gas in the growth process, which is set by the total pressure and the mole fraction of the feedstock, could be the factor that controls the thickness of the graphene. A series of experiments with continual and precisely controlled total pressure and ratio of growth gases was performed to generate a coherent growth map, as shown in Supporting Information, Table S2.

RESULTS AND DISCUSSION

As shown in Figure 1, a needle valve was installed between the CVD growth chamber (a quartz tube) and the vacuum pump to precisely control the gas flow rate and thus the total pressure of the CVD system. The total pressure was carefully monitored with a pressure gauge connected to the growth chamber. In Supporting Information, Table S2, a monolayer graphene growth condition was set as the first data point in the series, Sample 1. The growth reaction was maintained at 1000 °C for 15 min. The flow rates of H_2 and CH_4 were 300 sccm and 10 ± 1 sccm, respectively. The flow rates were kept the same throughout this series (Samples 1−12). The ratio between H_2 and CH_4 was thus fixed, while the total pressure was tuned from 5.8 to 740 Torr, ranging from low pressure growth to near-atmospheric pressure growth. The partial pressures of H_2

* Address correspondence to tour@rice.edu.

Received for review July 24, 2012 and accepted October 30, 2012.

Published online October 30, 2012
10.1021/nn303328e

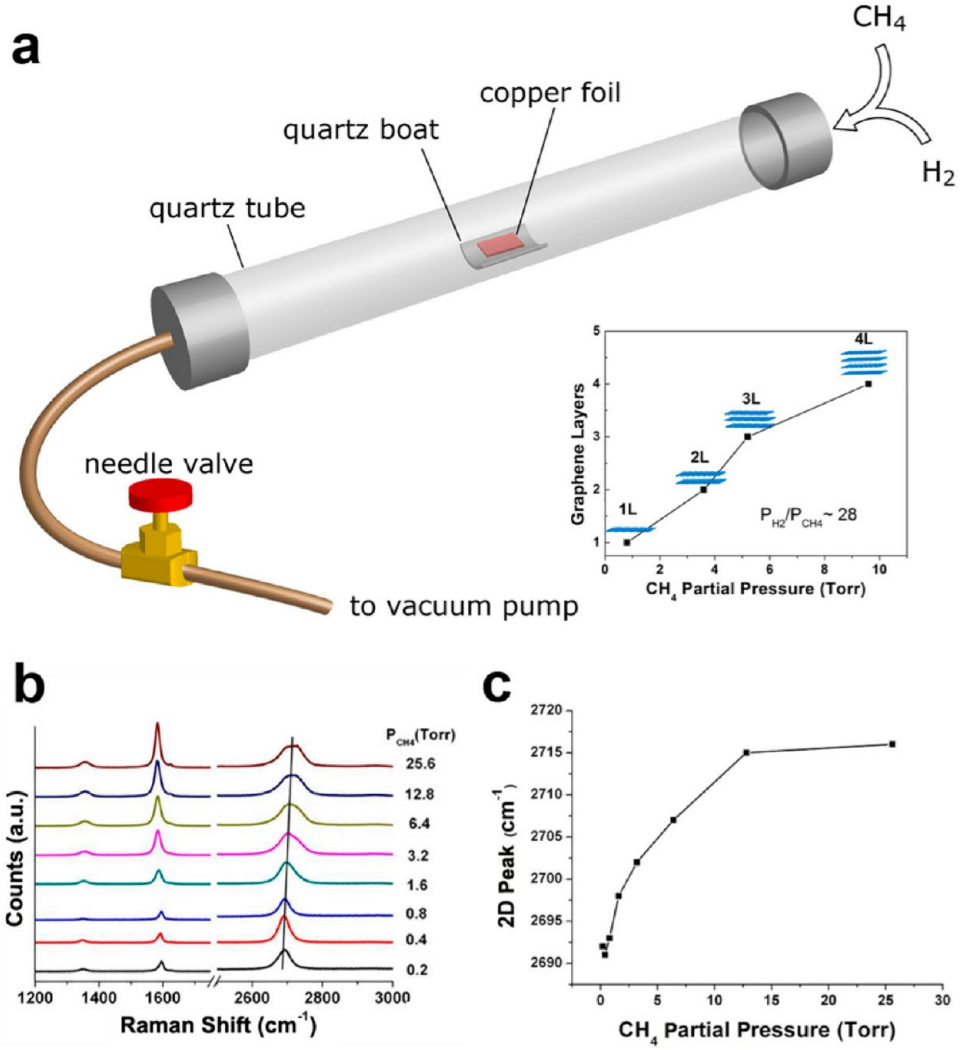

Figure 1. The growth chamber with a needle value to control the system pressure. (a) Scheme of the CVD growth chamber where a needle valve is placed downstream between the quartz tube and the vacuum pump to control the total pressure of CH_4 and H_2; the ratio of the two gases is controlled using mass flow controllers at the source of each gas. The growth chamber is placed in a furnace heated at 1000 °C. The inset is the partial pressure of CH_4 correlated to the thickness of the graphene layers. The ratio between partial pressure of H_2 (P_{H2}) and CH_4 (P_{CH4}) in this system was set by fixing the flow rates. (b) Raman evolution of graphene grown under increased CH_4 partial pressure (514 nm laser). (c) The 2D peak position of Raman spectra in panel b.

and CH_4 were calculated from the total system pressure. The detailed growth parameter values are listed in Supporting Information, Table S2. As the growth pressure increased, thicker graphene films grew on the Cu surfaces. Specifically, bi-, tri-, and tetralayer graphene films form when the P_{CH4} was 3.6, 5.2, and 9.6 Torr, respectively (inset of Figure 1a).

All of the graphene films were grown and transferred onto different substrates using the method previously described.[12] Optical images of this series transferred onto quartz slides are shown in Supporting Information, Figure S1. The graphene films became successively darker, suggesting that thicker films were grown with increasing P_{CH4}. The thickness of the films was subsequently investigated using spectroscopic techniques. Raman spectroscopy was used to determine both the quality and thickness of the graphene film over a micrometer-sized area according to the laser spot-size. On the basis of the Raman spectra in Figure 1b, when the P_{CH4} is below 1.6 Torr, only monolayer graphene films grow with an I_{2D}/I_G ratio less than 0.5 (Samples 1−3). At 1.6 Torr, bilayer graphene starts to form on Cu surfaces as the average I_G/I_{2D} increases to ~0.5, slightly higher than monolayer grapheneI_G/I_{2D} ratio.[13] Sample 4 is a hybrid of mono- and bilayer graphene film as confirmed by optical absorption of ~3%. When P_{CH4} was 3.6−3.8 Torr, Sample 5, the graphene film displays a dominant bilayer characteristic I_G/I_{2D} ratio over a large area.[5,14−16] Thicker graphene Raman signatures (3−10 layers) are also observed on the graphene films from Samples 6−10. Figure 1b displays the stacked Raman spectra as the P_{CH4} increased; the G peak at ~1585 cm^{-1} becomes more pronounced and the 2D peak at ~2700 cm^{-1}

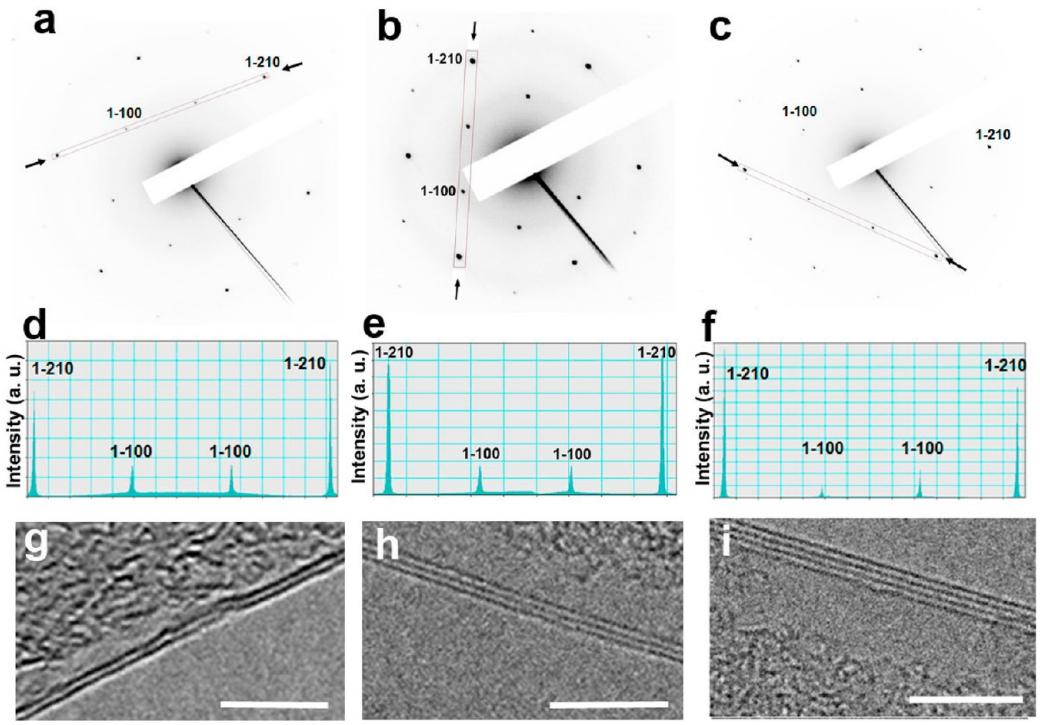

Figure 2. SAED and TEM characterization of bi-, tri-, and tetralayer graphene. (a−c) Representative SAED patterns from bi-, tri-, and tetralayer graphene samples, respectively. (d−f) The intensity profile from the SAED patterns in panels a−c, respectively. (g−i) High resolution TEM of randomly chosen representative edges of bi-, tri-, and tetralayer graphene that shows two, three, or four layers of carbon, respectively. Scale bar in panels g−i is 5 nm.

broadens and blueshifts.[17,18] In Figure 1c, the 2D peak-blueshift starts at 2690 cm^{-1} for monolayer graphene and ends at ~2717 cm^{-1} for >10-layer graphene, or graphite, which is consistent with the results obtained from mechanical exfoliated Bernal graphene.[13] The Raman spectra of non-Bernal stacked graphene were also investigated by directly stacking monolayer CVD graphene films atop a SiO_2 surface without further annealing. As shown in Supporting Information, Figure S2, both the I_{2D} and I_G increase as the thickness increases, while the relative ratio between the two peaks does not change, suggesting a relatively weak electronic interaction between graphene layers.[1,18] The deconvolution of the 2D peaks of bi-, tri-, and tetralayer graphene unveils more details, as shown in Supporting Information, Figure S3.[16] The 2D peak of bilayer graphene can be fitted with four Lorentzian curves while the 2D peak in trilayer graphene can be fitted with six Lorentzian curves. The line shape of the peak shows little asymmetry with no obvious shoulder, which suggests that the graphene films are dominated by Bernal (ABA) stacking order rather than rhombohedral (ABC) stacking order.[19] The tetralayer graphene's 2D peak can be fitted with 3 Lorentzian curves and its symmetrical line shape reveals its Bernal (ABAB) stacking signature. The full width at half-maximum values (FWHMs) of the 2D peaks are 62, 71, and 72 cm^{-1} in bi-, tri-, and tetralayer graphene, respectively, which are significantly broader than the fwhm of monolayer graphene at 30 cm^{-1}. All Raman spectra were acquired using a 514 nm laser at room temperature on SiO_2/Si substrates.

Selected area electron diffraction (SAED) patterns and high resolution transmission electron microscopy (HRTEM) images corroborate graphene's stacking order and thickness. Bi-, tri-, and tetralayer graphene films were carefully transferred onto TEM grids (C-flat, Electronmicroscopy Services). Over ~2 mm^2, ~10 SAED patterns were acquired per sample, and each area showed one set of diffraction pattern characteristic of Bernal stacking, other than at the grain boundaries. In the SAED patterns, the (1−210) intensity was 3.5−6.3 times stronger than the (1−100) in Figure 2a−f, suggesting that these films are non-AA stacked.[20] As a reference, the monolayer graphene diffraction pattern has a (1−210)/(1−100) intensity ratio of ~0.87 (Supporting Information, Figure S4). The presence of the innermost diffraction spots (1−100) and the diffraction intensity ratio in Figure 2 is quite different from the ABC stacking order, which should have an intensity ratio larger than 14 according to theoretical calculations.[20] However, experimental data do not always agree with theoretical diffraction data.[20] The inner plane strain and small tilting angle from the imperfect wet-transfer method could affect the diffraction intensities. Using the SAED patterns, the graphene films are Bernal (AB) stacked polycrystalline graphene with an average domain size of 1−5 μm; this result has the potential to be optimized into a single crystal using newly developed methods.[8] In Figure 2g−i, edges were randomly chosen for imaging

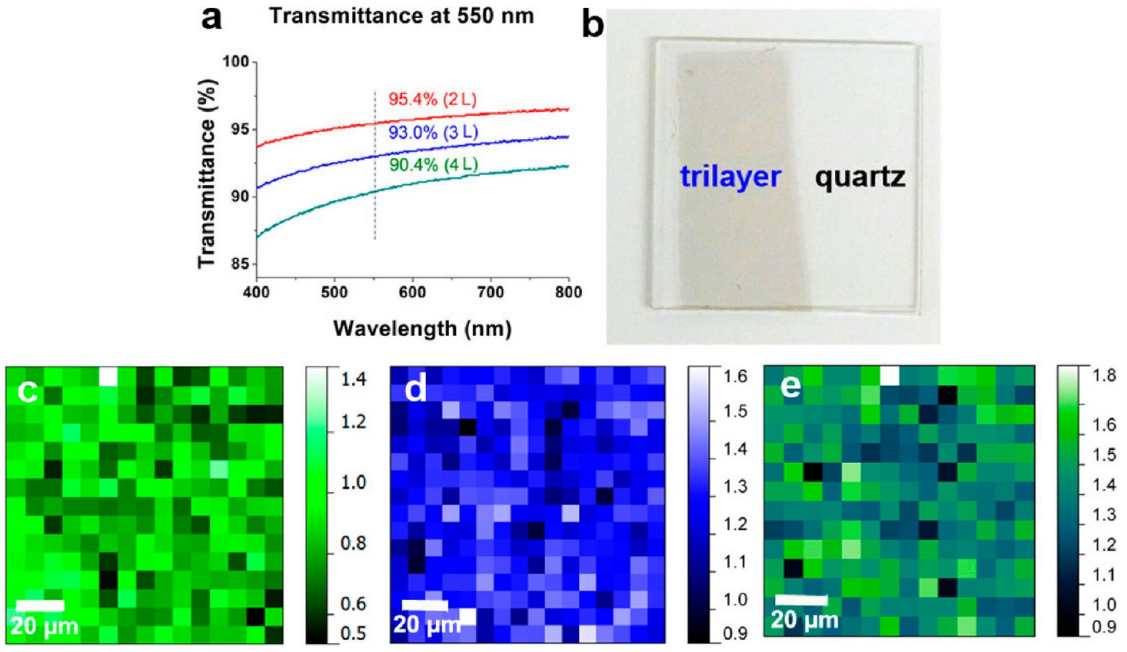

Figure 3. Spectroscopic characterization of Bernal bi-, tri-, and tetralayer graphene films. (a) Transmittance of bi-, tri-, and tetralayer graphene films obtained with visible-absorption spectroscopy on quartz substrates. The transmittance of graphene was measured at 550 nm. "*n* L" signifies the number of graphene layers. (b) Optical image of a trilayer graphene on 2.5 × 2.5 cm^2 quartz that indicates the uniformity of the film. I_G/I_{2D} Raman mapping of (c) bilayer, (d) trilayer, and (e) tetralayer graphene.

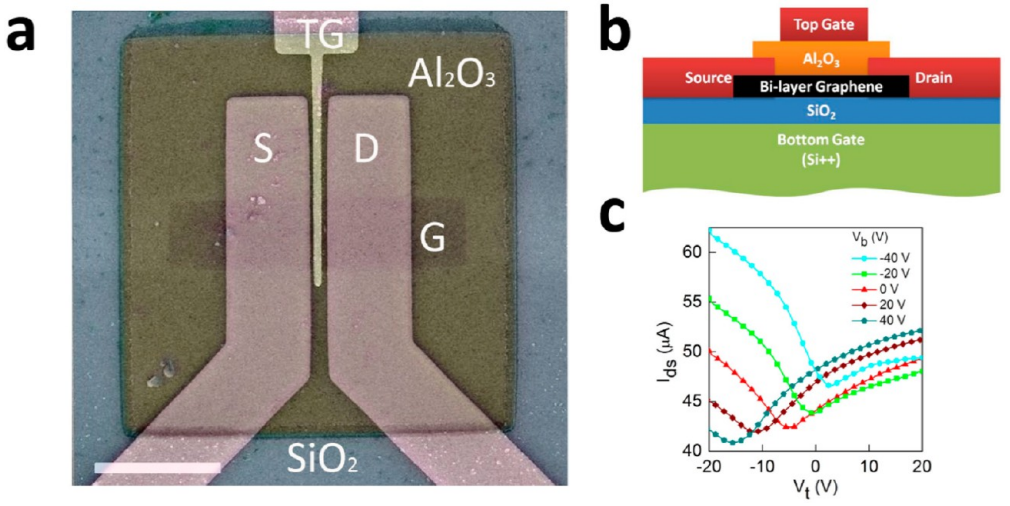

Figure 4. Electrical measurement of Bernal-stacked bilayer graphene. (a) Overlaid SEM and optical microscopy top-view image of a dual-gate bilayer graphene FET device (TG = top gate; G = bottom gate; S = source; D = drain). Scale bar is 10 μm. (b) Cross-sectional view of the bilayer graphene device. (c) Graphene electrical conductance as a function of top gate voltage V_t at different fixed bottom gate voltages V_b. The measurements were taken from −40 to 40 V in V_b, with 20 V steps at 77 K.

to confirm the thickness of the bi-, tri-, and tetralayer graphene samples.

The thickness of the graphene films was evaluated using visible spectroscopy in Figure 3a. At 550 nm, the bi-, tri-, and tetralayer graphene films on quartz substrates exhibit transmittances of 95.4%, 93.0%, and 90.4%, respectively, in good agreement with predicted and reported values.[21] Figure 3b shows no difference in contrast across the trilayer graphene film, providing evidence for the uniformity of the film. Statistically, Raman mapping at the 100 × 100 μm^2 scale confirms the thickness and uniformity of graphene films. In a typical monolayer graphene film, more than 95% of the graphene area has an I_G/I_{2D} ratio <0.5 (Supporting Information, Figure S5). In Figure 3c, no monolayer Raman signature (I_G/I_{2D} < 0.5) was observed at any pixel on the map and ~85% of the film had an I_G/I_{2D} ratio of 0.7−1.1, suggesting uniform bilayer graphene.[18] The Raman 2D band has been shown to be sensitive to graphene interlayer coupling, whereby ordered

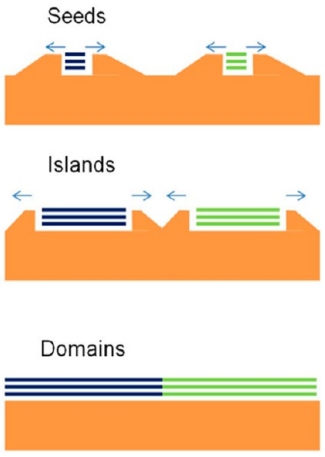

Figure 5. Proposed growth-mechanism. Graphene seeds form when the surface carbon in Cu is supersaturated. Higher CH_4 partial pressure deposits thicker graphene seeds. The thickness of the graphene is predefined by these seeds, which grow epitaxially along the Cu surface (top). The graphene seeds grow independently and form graphene single-crystalline islands (middle) before they meet with each other. When graphene islands meet, they form domains and grain boundaries (bottom) and the growth stops. No additional graphene layer would be able to grow on the fully covered Cu surface.

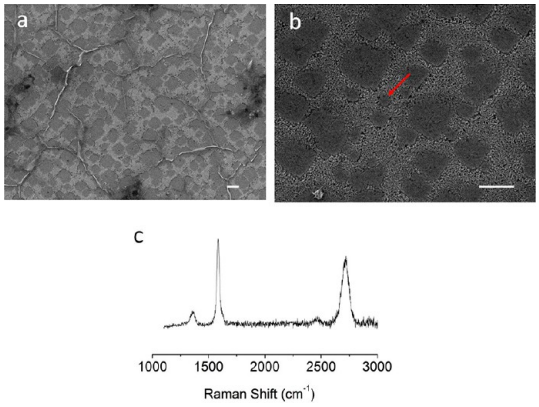

Figure 6. Panels a and b are different magnification SEM images of bilayer graphene seeds and islands after 2 min growth atop Cu. The Cu foil is prepolished and annealed using the same method discussed in ref 24. This additional treatment is necessary to minimize carbon contamination on the Cu surface. Without this treatment, the full coverage of graphene growth finished too quickly for the seeds to be arrested and captured. The red arrow in panel b points to a graphene seed. This graphene seed is surrounded with graphene islands, which range from 100 nm to several μm in size (here, seeds are simply small islands). The scale bar in panels a and b is 1 μm. (c) Representative Raman spectrum of these bilayer graphene seeds and islands, which shows the same signature as its final bilayer film. Out of 10 random areas studied, eight areas were bilayer while one area was monolayer and another was trilayer. This indicates that the seeds were mainly bilayer.

few-layer graphene exhibits 2D band-broadening in addition to a shift to higher frequency.[19] In Supporting Information, Figure S6, ~85% of the sample's fwhm 2D peak falls within 42.5 cm^{-1} and 62.5 cm^{-1}, characteristic of strongly coupled bilayer graphene.[22] Substrate effects or incidental charging could contribute to the deviation in the ratio. In Figure 3d,e, the average I_G/I_{2D} ratios were 1.29 (trilayer) and 1.44 (tetralayer), respectively. This result was similar to tri- and tetralayer Bernal-stacked exfoliated graphene (obtained from highly oriented pyrolytic graphite), while it is different than the previous values for CVD-grown graphene.[1,18]

Dual-gate field effect transistors (FETs) were built with a bilayer graphene film atop a SiO_2/Si wafer (Figure 4). The electrical measurements on the devices indicate that they have a tunable band structure with a biased electrical field perpendicular to the graphene basal plane.[1−4] The device hole mobility was as high as ~2200 cm^2 V^{-1} s^{-1} (Supporting Information, Figure S7), which is considerably higher than the mobility for solution-exfoliated Bernal bilayer graphene.[23]

Additional control experiments were done to explore the growth mechanism for the Bernal stacked graphene films. Under bilayer growth conditions (Sample 5 in Supporting Information, Table S2), 15-min-growth produces full coverage of a bilayer graphene film on the Cu surface. Extending the growth time to 30 min under the same conditions does not change the film's thickness (Supporting Information, Figure S8). In addition, monolayer graphene was grown to fully cover the Cu surface, after which the CVD system was changed to a higher pressure favorable for bilayer growth. However, no additional growth was observed (Supporting Information, Figure S9). This confirmed that the graphene growth is not a layer-by-layer mechanism, in which an additional graphene film can grow directly atop or underneath existing graphene film. The polycrystalline nature indicates that the graphene is grown from multiple growth centers and that the crystals subsequently merge seamlessly. The growth of the Bernal stacked graphene suggests that a self-limiting mechanism is operating and that the thickness is inherent from its early seeding stage.

The proposed growth-mechanism scheme is shown in Figure 5. In a concentrated carbon species growth environment, multilayer graphene seeds form when C atoms are supersaturated in the surface layers of the Cu. To arrest the intermediate states, a short time-growth (2 min) on pretreated Cu surface was performed. The Cu foil was prepolished and annealed using the same method discussed elsewhere.[24] In Figure 6, the SEM and Raman spectra clearly confirmed that the graphene thickness was defined at the initial stage. Considering the top graphene layers have no direct lateral contact with the Cu underneath except for the edges, this two-dimensional growth is most likely catalyzed by the Cu catalyst-front close to the graphene edges as shown in Figure 5. In this way, some of the seeds grow into graphene islands, forming and extending synchronously rather than layer-by-layer. The islands maintain their thickness and stacking order while the edges propagate laterally on the Cu surface. In analogy to the "tip-growth" mechanism of carbon

nanotubes,[25] the growth of Bernal graphene is most likely following an "edge-growth" mechanism. Cu "wave fronts" are pushed back into the surface by growing graphene crystals or they evaporate from this surface mobile state. As the graphene islands expand, the open Cu area shrinks. Finally, two graphene domains merge into one, with no Cu front left in between. As the growth temperature is close to copper's melting point, the front of the catalyst could be a highly mobile liquid phase. This mechanism is proposed for Bernal-stacked graphene growth. But it could be generalized for all 2D graphitic growth on Cu, including monolayer graphene and graphite (>10 layers). With the same mechanism, Bernal-stacked graphite of more than 10 graphene layers could be produced from Cu substrates (Supporting Information, Figure S10).

CONCLUSIONS

We have shown here that between 1 and 4 layers, the thickness of Bernal-stacked graphene, can be tuned within selective growth windows. Indications suggest the same type of growth up to 10 layers thick. A defined-seed mechanism is proposed that yields the precise layer thickness of the final graphene films. These Bernal-stacked graphene films are expected to show distinct electronic band structures, adding new building blocks to existing graphene catalogs and promoting physical and optoelectronic applications.[26]

EXPERIMENTAL SECTION

CVD Growth. In a 48-in. long fused quartz tube (22-mm ID, 25-mm OD, Technical Glass Products) heated in a furnace, graphene films were grown on a ~ 1 in^2 copper foil mounted on a boat-shaped quartz holder with a magnet affixed at one end to facilitate insertion and removal (the magnet never enters the hot-zone of the oven). With the furnace heated to 1000 °C and the tube under vacuum (<30 mTorr), filtered H_2 (ultrahigh purity grade, 99.999% from Matheson, this high purity cannot be substituted) was introduced at 300 sccm and the H_2 pressure was controlled with a needle valve (Figure 1a) to a specified value. The copper foil was then annealed for 10 min by sliding the holder containing the copper to the center of the furnace. In the presence of the pressure-controlled H_2, filtered methane (chemical purity grade, 99.0%, Matheson) was opened at 10 ± 1 sccm for a growth time of 15 min after which the holder was removed from the furnace area of the tube to cool under H_2. The copper foil was 25 μm thick and 99.8% grade, purchased from Alfa Aesar.

Transfer. Graphene was formed on both sides of the Cu foil. To protect the graphene film during Cu etching, a poly(methyl methacrylate) (PMMA) solution (950 PMMA A 4, MicroChem) was spin-coated (at 2500 rpm for 1 min) on the top of the graphene-coated copper foil twice and baked at 70 °C for ~30 min in a vacuum oven or on a hot plate.[1] Marble's reagent was used as an aqueous etchant solution, comprising 15.6 g of $CuSO_4 \cdot 5H_2O$ (Aldrich), 45 mL of deionized H_2O, and 50 mL of concn HCl (Aldrich). The PMMA−graphene−Cu assembly was etched for a few min after which the Cu foil was removed from the Marble's reagent and dipped in water several times and wiped on a Kimwipe to completely remove the unprotected graphene on the bottom of the Cu foil so that its residue did not merge with the top graphene. The remaining Cu was etched, leaving the PMMA-protected graphene that had been on top of the Cu foil floating on the etchant. The film was floated on deionized water and subsequently transferred onto a given substrate; the protective PMMA was removed using acetone after the transferred graphene layer completely dried. The graphene film was rinsed with 2-propanol, and gently blow-dried using N_2.

Characterization. For Raman spectroscopy, scanning electron microscopy (SEM), and optical characterization, graphene films were transferred onto a 300 nm SiO_2/Si substrate. Raman spectra and 2D Raman maps were collected using a Renishaw inVia Raman microscope with a 514 nm Ar laser at ambient temperature. SEM images were obtained with a JEOL 6500F SEM at 15 KV. Optical images were taken with a Zeiss Axioplan Polarized Optical Microscope. On quartz slides, optical transmittance spectra were collected in a Shimadzu UV-3101PC UV−vis−NIR spectrophotometer. Transmission electron microscopy (TEM) images and electron diffraction patterns were acquired using a JEOL 2100F field emission gun TEM at 200 kV. The diffraction patterns were obtained at 80 000× with a zero degree tilt. For the TEM experiments, graphene films were transferred onto C-flat TEM grids (Electron Microscopy Sciences) in a method similar to the transfer method used for silicon oxide substrates.

Electrical Measurement. The bilayer graphene sheet was transferred to p-Si substrates with 300 nm thermal oxide and patterned into a strip (5×20 μm) using ebeam lithography and reactive ion etching (RIE). The source/drain electrodes (1 nm Ti/20 nm Au) were defined using ebeam lithography and ebeam evaporation. Then top gate dielectrics (alumina, 70 nm) and top gate electrode (1 nm Ti/20 nm Au) were defined in series using ebeam lithography and ebeam evaporation. The channel length was between 1 and 5 μm depending on the devices.

The dual-gate FET properties of the bilayer graphene devices were further characterized using a probe station (Desert Cryogenics TTPX-probe 6 system) under vacuum with chamber base pressure below 1×10^{-5} mm Hg. The I−V data were collected using an Agilent 4155C semiconductor parameter analyzer.The mobility was calculated using the following equation:

$$\mu = \frac{L}{WC_{ox}V_{sd}} \frac{\Delta I_{sd}}{\Delta V_g}$$

where L and W are the channel length and width, C_{ox} is the gate oxide capacitance, V_{sd} is the source drain voltage, I_{sd} is the source drain current, and V_g is the gate voltage. The linear regime of the transfer characteristics was used to obtain $\Delta I_{sd}/\Delta V_g$.

Conflict of Interest: The authors declare no competing financial interest.

Acknowledgment. This work was funded by the AFOSR (FA9550-09-1-0581), the AFOSR MURI (FA9550-12-1-0035), the Lockheed Martin Corporation through the LANCER IV Program, and the ONR MURI Program (No. 00006766, N00014-09-1-1066).

Supporting Information Available: Optical photograph of graphene films, Raman spectra of monolayer and non-Bernal-stacked graphene films, 2D band fitting for bi-, tri-, and tetralayer films, Raman mapping and SAED pattern of monolayer graphene, FET device measurement and $I-V$ curve, experimental details for proposed growth-mechanism, HRTEM image of graphite film, tables of CVD growth conditions both from the literature and the one developed in this work. This material is available free of charge *via* the Internet at http://pubs.acs.org.

REFERENCES AND NOTES

1. Reina, A.; Jia, X.; Ho, J.; Nezich, D.; Son, H.; Bulovic, V.; Dresselhaus, M. S.; Kong, J. Large Area, Few-Layer Graphene Films on Arbitrary Substrates by Chemical Vapor Deposition. *Nano Lett.* **2009**, *9*, 30–35.

2. Kim, K. S.; Zhao, Y.; Jang, H.; Lee, S. Y.; Kim, J. M.; Kim, K. S.; Ahn, J.; Kim, P.; Choi, J.; Hong, B. H. Large-Scale Pattern Growth of Graphene Film for Stretchable Transparent Electrodes. *Nature* **2009**, *457*, 706–710.
3. Li, X.; Cai, W.; An, J.; Kim, S.; Nah, J.; Yang, D.; Piner, R.; Velamakanni, A.; Jung, I.; Tutuc, E.; *et al.* Large-Area Synthesis of High-Quality and Uniform Graphene Films on Copper Foils. *Science* **2009**, *324*, 1312–1314.
4. Ohta, T.; Bostwick, A.; Seyller, T.; Horn, K.; Rotenberg, E. Controlling the Electronic Structure of Bilayer Graphene. *Science* **2006**, *313*, 951–954.
5. Oostinga, J. B.; Heersche, H. B.; Liu, X.; Morpurgo, A. F.; Vandersypen, L. M. K. Gate-Induced Insulating State in Bilayer Graphene Devices. *Nat. Mater.* **2007**, *7*, 151–157.
6. Craciun, M. F.; Russo, S.; Yamamoto, M.; Oostinga, J. B.; Morpurgo, A. F.; Tarucha, S. Trilayer Graphene Is a Semimetal with a Gate-Tunable Band Overlap. *Nat. Nanotechnol.* **2009**, *4*, 383–388.
7. Zhang, Y.; Tang, T.; Girit, C.; Hao, Z.; Martin, M. C.; Zettl, A.; Crommie, M. F.; Shen, Y. R.; Wang, F. Direct Observation of a Widely Tunable Bandgap in Bilayer Graphene. *Nature* **2009**, *459*, 820–823.
8. Yu, Q.; Jauregui, L. A.; Wei, W.; Colby, R.; Tian, J.; Su, Z.; Cao, H.; Liu, Z.; Pandey, D.; Wei, D.; *et al.* Control and Characterization of Individual Grains and Grain Boundaries in Graphene Grown by Chemical Vapour Deposition. *Nat. Mater.* **2011**, *10*, 443–449.
9. Bhaviripudi, S.; Jia, X.; Dresselhaus, M. S.; Kong, J. Role of Kinetic Factors in Chemical Vapor Deposition Synthesis of Uniform Large Area Graphene Using Copper Catalyst. *Nano Lett.* **2010**, *10*, 4128–4133.
10. Li, X.; Magnuson, C. W.; Venugopal, A.; An, J.; Suk, J. W.; Han, B.; Borysiak, M.; Cai, W.; Velamakanni, A.; Zhu, Y.; et al. Graphene Films with Large Domain Size by a Two-Step Chemical Vapor Deposition Process. *Nano Lett.* **2010**, *10*, 4328–4334.
11. Lee, S.; Lee, K.; Zhong, Z. Wafer Scale Homogeneous Bilayer Graphene Films by Chemical Vapor Deposition. *Nano Lett.* **2010**, *10*, 4702–4707.
12. Sun, Z.; Yan, Z.; Yao, J.; Beitler, E.; Zhu, Y.; Tour, J. M. Growth of Graphene from Solid Carbon Sources. *Nature* **2010**, *468*, 549–552.
13. Ferrari, A. C.; Meyer, J. C.; Scardaci, V.; Casiraghi, C.; Lazzeri, M.; Mauri, F.; Piscanec, S.; Jiang, D.; Novoselov, K. S.; Roth, S.; *et al.* Raman Spectrum of Graphene and Graphene Layers. *Phys. Rev. Lett.* **2006**, *97*, 187401.
14. Ni, Z. H.; Wang, H. M.; Kasin, J.; Fan, H. M.; Yu, T.; Wu, Y. H.; Feng, Y. P.; Shen, Z. X. Graphene Thickness Determination Using Reflection and Contrast Spectroscopy. *Nano Lett.* **2007**, *7*, 2758–2763.
15. Yacoby, A. Graphene: Tri and Tri Again. *Nat. Phys.* **2011**, *7*, 925–926.
16. Malard, L. M.; Pimenta, M. A.; Dresselhaus, G.; Dresselhaus, M. S. Raman Spectroscopy in Graphene. *Phys. Rep.* **2009**, *473*, 51–87.
17. Yoon, D.; Moon, H.; Cheong, H. Variations in the Raman Spectrum as a Function of the Number of Graphene Layers. *J. Korean Phys. Soc.* **2009**, *55*, 1299–1303.
18. Hao, Y. F.; Wang, Y.; Wang, L.; Ni, Z.; Wang, Z.; Wang, R.; Koo, C. K.; Shen, Z.; Thong, J. T. L. Probing Layer Number and Stacking Order of Few-Layer Graphene by Raman Spectroscopy. *Small* **2010**, *6*, 195–200.
19. Lui, C. H.; Li, Z.; Chen, Z.; Klimov, P. V.; Brus, L. E.; Heinz, T. Imaging Stacking Order in Few-Layer Graphene. *Nano Lett.* **2011**, *11*, 164–169.
20. Horiuchi, S.; Gotou, T.; Fujiwara, M.; Sotoaka, R.; Hirata, M.; Kimoto, K.; Asaka, T.; Yokosawa, T.; Matsui, Y.; Kenji, W.; *et al.* Carbon Nanofilm with a New Structure and Property. *Jpn. J. Appl. Phys.* **2003**, *42*, 1073–1076.
21. Bae, S.; Kim, H.; Lee, Y.; Xu, X.; Park, J.; Zheng, Y.; Balakrishnan., J.; Lei, T.; Kim, H. R.; Song, Y. I.; *et al.* Roll-to-Roll Production of 30-in. Graphene Films for Transparent Electrodes. *Nat. Nanotechnol.* **2010**, *5*, 574–578.
22. Chen, S.; Cai, W.; Piner, R. D.; Suk, J. W.; Wu, Y.; Ren, J.; Kang, J.; Ruoff, R. S. Synthesis and Characterization of Large-Area Graphene and Graphite Films on Commercial Cu–Ni Alloy Foils. *Nano Lett.* **2011**, *11*, 3519–3525.
23. Shih, C. J.; Vijayaraghavan, A.; Krishnan, R.; Sharama, R.; Han, J.; Ham, M.; Jin, Z.; Lin, S.; Paulus, G. L. C.; Reuel, N. F.; *et al.* Bi- and Trilayer Graphene Solutions. *Nat. Nanotechnol.* **2011**, *6*, 439–445.
24. Yan, Z.; Lin, J.; Peng, Z.; Sun, Z.; Zhu, Y.; Li, L.; Xiang, C.; Samuel, E. L.; Kittrell, C.; Tour, J. M. Towards the Synthesis of Wafer-Scale Single-Crystal Graphene on Copper Foils. *ACS Nano* **2012**, *6*, 9110–9117.
25. Charlier, J. C.; Amara, H.; Lambin, P. Catalytically Assisted Tip Growth Mechanism for Single-Wall Carbon Nanotubes. *ACS Nano* **2007**, *1*, 202–207.
26. Bonaccorso, F.; Sun, Z.; Hasan, T.; Ferrari, A. C. Graphene Photonics and Optoelectronics. *Nat. Photon.* **2010**, *4*, 611–622.